Available online at www.sciencedirect.com
SCIENCE DIRECT
International Journal of Heat and Mass Transfer 49 (2006) 4437–4443
International Journal of HEAT and MASS TRANSFER
www.elsevier.com/locate/ijhmt

Molecular dynamics simulation on bubble formation in a nanochannel

Gyoko Nagayama [a,*], Takaharu Tsuruta [a], Ping Cheng [b]

[a] Department of Mechanical Engineering, Kyushu Institute of Technology, 1-1 Sensui, Tobata, Kitakyushu 804-8550, Japan
[b] School of Mechanical and Power Engineering, Shanghai Jiaotong University, 1954 Hua-Shan Road, Shanghai 200030, China

Received 4 November 2005; received in revised form 29 April 2006
Available online 3 July 2006

Abstract

Molecular dynamics simulations are carried out to examine the bubble behavior confined in a nanochannel with particular emphasis on the nucleation phenomenon. Simple Lennard-Jones fluids are under consideration and nano-sized bubbles are observed under different conditions of solid–liquid interfacial wettability. It is found that the bubble nucleation behavior shows a marked dependence on the solid–liquid interfacial interaction. In particular, it is found that bubbles appear in the bulk liquid homogenously for a hydrophilic surface, but grow directly on a hydrophobic solid surface. Also, a bubble will not form on a non-wetting surface. A nanobubble exists stably under the equilibrium state and the number density distribution of the curved liquid–vapor interface is examined. It is also found that there are few vapor atoms in the nano-sized bubble and the internal vapor pressure of the nanobubble is much lower than that required from the Young–Laplace equation. The disagreement with the prediction of the Young–Laplace equation can be attributed to the fact that the liquid–vapor interface region plays an important role on the force balance at the curved liquid–vapor interface of a nanobubble.

Keywords: Nanobubble; Young–Laplace equation; Liquid–vapor interface; Molecular dynamics simulation; Nucleation

1. Introduction

The study of bubble dynamics in the microscale thermo-fluidic flow has attracted considerable attention recently owing to rapid advances in micro-electronic fabrication technologies. In a microsystem, effect of solid surface is very important and the interface resistance between liquid and solid plays a dominant role. For single phase flow in a microchannel, recent studies [1,2] have shown that the surface wettability affects the heat transfer characteristics because it changes the interfacial structure and the activities of fluid molecules adjacent to the solid surface. With increasing heat flux in a micro-heat exchanger using phase change working media, bubble formation may occur and a two-phase flow results [3–5]. From a classical point of view, however, the formation of nano-size bubble needs much higher superheat [6,7]. It appears that there is considerable controversy as to exactly how bubbles are formed initially on a solid surface. The mechanism is still unclear.

For bubble nucleation in a pure liquid phase, extensive works have been done from a molecular scale as well as the classical point of view [8–16]. Kinjo and Matsumoto [11] have carried out molecular dynamics simulations for cavitation processes under negative pressure, and found that the nucleation rate is 8 orders of magnitude larger than that of the classical nucleation theory. Maruyama and Kimura [8] studied heterogeneous nucleation on a solid surface and they found that the classical nucleation theory can predict the results obtained by their molecular dynamics simulation results. Kinjo et al. [13] have conducted molecular dynamics simulation for homogeneous nucleation or heterogeneous nucleation on a hydrophilic and a hydrophobic surface. However, a fully understanding about how bubbles are initially formed near the solid surface has not been presented.

* Corresponding author. Tel./fax: +81 93 884 3139.
E-mail address: nagayama@mech.kyutech.ac.jp (G. Nagayama).

0017-9310/$ - see front matter © 2006 Elsevier Ltd. All rights reserved.
doi:10.1016/j.ijheatmasstransfer.2006.04.030

Nomenclature

D	distance between two walls from the first solid layer	σ	surface tension (without subscripts)
h_{fg}	entropy of evaporation	σ	length parameter of LJ potential
L	size of simulation system	ε	energy parameter of LJ potential
P	pressure	v'	specific volume of liquid
r	radius of the bubble	v''	specific volume of vapor
r_{ij}	distance between molecule i and j	ΔT_s	super heat
T	temperature	θ	contact angle
T_w	wall temperature	ρ	density
		ϕ	potential energy

Greek symbols

α	potential energy factor to adjust the strength of hydrophilic interaction
β	potential energy factor to adjust the attraction for hydrophobic interaction

Subscripts

l	liquid
s	solid
sat	saturation
v	vapor

In this paper, we examine the bubble formation in a nanochannel with particular emphasis on the effect of solid–liquid interfacial wettability on nucleation phenomenon. An examination of nanobubble formation based on molecular dynamics of a simple Lennard-Jones fluid will provide useful information concerning bubble nucleation on solid surfaces. A metastable liquid confined in a nanochannel with an inlet driving force is simulated. A modified Lennard-Jones potential function is utilized to represent different solid–liquid interfacial interaction by adjusting the potential parameters. The bubble formation behavior is thus examined by changing the magnitudes of the driving force and the solid–liquid interfacial wettability. It is shown that there is a significant difference between the hydrophilic surface and the hydrophobic surface on the type of nucleation occurring. For a hydrophilic surface, bubbles are generated in the bulk liquid homogenously. In the case of a hydrophobic surface, heterogeneous nucleation is observed, i.e., bubbles appear on the solid surface directly. Apparent velocity slip occurs at the boundary in this case. For a non-wetting surface, the results show that a gap exists between the liquid and the solid surface and no bubble appears in the nanochannel. It is also found that there are few vapor atoms in the nano-size bubble and the temperature or pressure inside bubble disagrees with the prediction of the macroscopic Young–Laplace equation.

2. Simulation methods

Molecular dynamics simulations are performed for liquid molecules confined in a nanochannel bounded by two planar solid walls in the canonical ensemble (NVT). Fig. 1 shows the simulation system, where the simulation cell has the size of $L_x = 5.83$ nm, $L_y = 3.85$ nm, $L_z = 7.22$ nm and the distance between two walls D is 5.41 nm. Each solid wall consists of four layers of atoms arranged

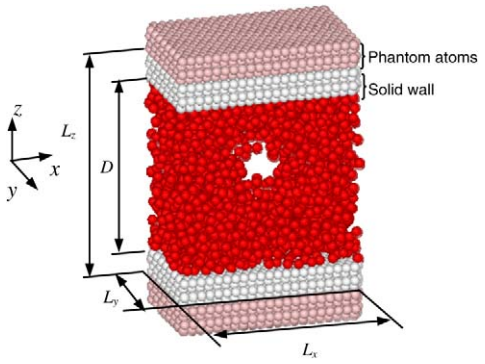

Fig. 1. Simulation system for bubble formation in the steady state.

as a FCC lattice and its ⟨1 1 1⟩ surface is in contact with the liquid. It is assumed that the solid walls are made of platinum and the Lennard-Jones fluid is argon. Periodic boundary conditions are applied along the x- and y-directions. In the z-direction, outside each solid wall of the simulation cell, four layers of phantom solid atoms anchored by their lattice are located to model a semi-infinite potential field of the solid wall [8]. For the geometry under consideration, there are 2688 solid atoms corresponding to the density of platinum, 21.45×10^3 kg/m^3. If the system temperature is maintained at 100 K and if the effect of the solid wall is ignored, the liquid saturation density corresponds to 2400 liquid argon atoms in the nanochannel. Simulations for 2400 atoms were performed in our previous work corresponding to an initial state with $\rho_l/\rho_{lsat} = 1$ where no bubble was observed [2]. In this paper, we carry out simulations at a temperature of 100 K on two different initial conditions: (i) 1440 argon atoms corresponding to $\rho_l/\rho_{lsat} = 0.600$, and (ii) 2000 argon atoms corresponding to $\rho_l/\rho_{lsat} = 0.833$. Fig. 2 shows the simulation points ($N_{Ar} = 1440$ and $N_{Ar} = 2000$) in comparison with the coexistence curve and the spinodal line [11] of bulk liquid for

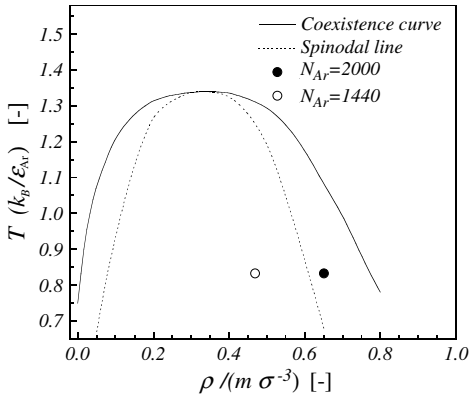

Fig. 2. Simulation points and phase diagram with coexistence curve and spinodal line.

reference, where the region between the coexistence curve and the spinodal line represents the metastable region. As discussed in a previous paper [2], the bulk liquid density should be influenced by the wall-boundaries. A decrease in the bulk liquid density is found at the hydrophilic surface but an increase is found at the hydrophobic surface. For the simulation point on the outside of the metastable region of the open circle ($N_{Ar} = 1440$), the bubble is found at both the hydrophilic wall surface and the hydrophobic wall surface from the initial condition without any driving force. The details are shown in later Sections 3.2 and 3.3. For the simulation point on the inside of the metastable region of the closed circle ($N_{Ar} = 2000$), no bubble has been observed from the initial condition without any driving force and the details are described in Sections 3.2 and 3.3. Therefore, the simulation points are in substantial agreement with those shown in Fig. 2.

All simulations were performed with a time step of 5 fs. A selected cut off radius of $3.5\sigma_l$ for the spherically truncated and shifted (STS) potential was used to simulate force field. The equations of motion were integrated by the Velocity Verlet algorithm [17].

An equilibrium system at 100 K from the initial state without liquid–solid interaction was first achieved. Then, simulations were carried out under different solid–liquid interfacial wettabilities for 5 ns to reach a steady equilibrium state. Non-equilibrium molecular dynamic simulation (NEMD) was then carried out from this equilibrium state.

In order to examine the bubble formation from a metastable state, we apply an external force at the inlet region of the channel. The external force is added to each particle located at the inlet and the length of the inlet region is defined as one atomic diameter of argon, which is about 4.7% of the channel length. Simulations with the driving force were carried out with a magnitude of 1.96 pN. Because the work of external driving force may lead to the generation of heat in the system, the simple velocity scaling technique [18] was applied to the outside layer of each wall (not all wall atoms) to maintain a constant wall temperature. Since the control of the system temperature was not applied to all wall atoms, it would allow the local temperature fluctuation in the channel if it occurred during nucleation process. Similarly, a constant inlet temperature of 100 K (the same as the wall) was applied to the liquid in the inlet region. It should be noted that no thermostat was coupled to liquid or solid elsewhere for all simulation cases.

Force field for molecular dynamics simulation was based on the Lennard-Jones (LJ) potential function. For the liquid–liquid interaction, the LJ potential was applied to argon with the length parameter $\sigma_l = 3.405$ Å, and the energy parameter $\varepsilon_l = 1.67 \times 10^{-21}$ J:

$$\phi_l(r_{ij}) = 4\varepsilon_l\left[\left(\frac{\sigma_l}{r_{ij}}\right)^{12} - \left(\frac{\sigma_l}{r_{ij}}\right)^{6}\right] \tag{1}$$

The LJ potential was also applied for the solid–solid interaction with $\sigma_s = 2.475$ Å corresponding to the lattice constant 2.776 Å of platinum, and $\varepsilon_s = 8.35 \times 10^{-20}$ J for the potential well depth of Pt–Pt:

$$\phi_s(r_{ij}) = 4\varepsilon_s\left[\left(\frac{\sigma_s}{r_{ij}}\right)^{12} - \left(\frac{\sigma_s}{r_{ij}}\right)^{6}\right] \tag{2}$$

The method of tethering the solid molecules to a fixed lattice site was not used and present energy parameter ε_s for Pt results in a good agreement with the frequency of vibration around the lattice site. For the solid–liquid interaction, a modified form of the LJ potential was used [2]. It is a combination of the potential models used by Din and Michaelides [19] as well as by Barrat and Bocquet [20]:

$$\phi_{sl}(r_{ij}) = 4\varepsilon_{sl}\left[\left(\frac{\sigma_{sl}}{r_{ij}}\right)^{12} - \beta\left(\frac{\sigma_{sl}}{r_{ij}}\right)^{6}\right], \tag{3}$$

where $\sigma_{sl} = (\sigma_l + \sigma_s)/2$, and the energy parameter ε_{sl} is given by $\varepsilon_{sl} = \alpha\sqrt{\varepsilon_l\varepsilon_s}$ based on the Lorentz–Berthelot combining rule [21]. Parameters α and β in Eq. (3) are used to adjust the strength of the hydrophilic interaction and the hydrophobic interaction. Details for the values of α and β setting will be reported in the next section.

3. Results and discussion

3.1. Solid–liquid interfacial wettabilities and contact angles

The parameters α and β of Eq. (3) with the corresponding values of the contact angle were obtained from simulations of droplet formation on a solid substrate. The simulation system illustrated in Fig. 3 consists of a solid substrate with 1344 platinum atoms and 500 argon atoms in an equilibrium state at 100 K. The simulation method is similar to the studies of Barrat and Bocquet [20] as well as Maruyama et al. [8–10].

Cases (a)–(c) are at $\beta = 1$ with the values of $\alpha = 1$ for (a), $\alpha = 0.5$ for (b), and $\alpha = \sqrt{\varepsilon_l/\varepsilon_s} = 0.14$ (i.e., $\varepsilon_{sl} = \varepsilon_l$) for (c). As shown in Fig. 3, Cases (a)–(c), the liquid molecules wet the solid surface well, which have zero contact angles. That is, the values of α and β for Cases (a)–(c) correspond to the hydrophilic surfaces. For the hydrophilic surface (a) with

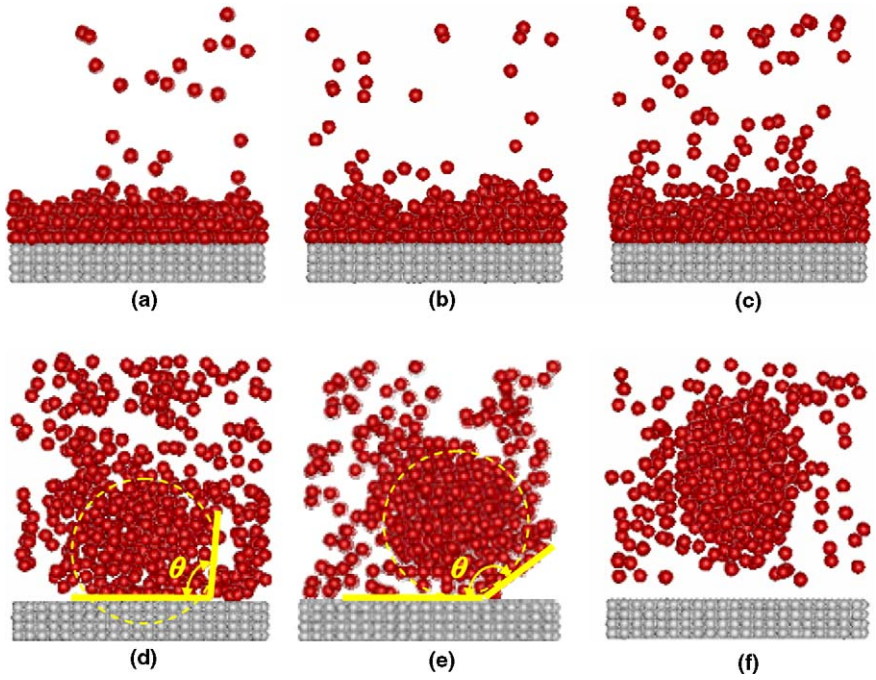

Fig. 3. Solid–liquid interface wettability and potential parameters α and β of Eq. (3). (a) $\alpha = 1$, $\beta = 1$; (b) $\alpha = 0.5$, $\beta = 1$; (c) $\alpha = 0.14$, $\beta = 1$; (d) $\alpha = 0.14$, $\beta = 0.5$; (e) $\alpha = 0.14$, $\beta = 0.3$; (f) $\alpha = 0.14$, $\beta = 0.1$.

$\alpha = 1$ and $\beta = 1$, it shows that the liquid molecules distribute orderly in the vicinity of the solid interface due to strong solid–liquid interactions. Three orderly layers attached to the solid surface can be seen in this case. With decreasing α, Case (b) ($\alpha = 0.5$) shows two orderly layers and Case (c) ($\alpha = 0.14$) shows only one layer. Therefore, parameters α and β for Cases (a)–(c) represent strong, middle and weak hydrophilic interactions, respectively.

Cases (d)–(f) are at $\alpha = \sqrt{\varepsilon_l/\varepsilon_s} = 0.14$, with different values of β. Fig. 3 shows that a droplet is formed on the substrate for the Cases (d)–(f), having contact angles of 95°(±5°), 150°(±5°) and 180°, respectively. We therefore define Cases (d)–(f) are hydrophobic surfaces, corresponding to the partial wetting and non-wetting situations. The values of $\beta = 0.5$ for (d), $\beta = 0.3$ for (e) and $\beta = 0.1$ for (f) represent weak, middle and strong hydrophobic interactions, respectively. Table 1 summarizes surfaces (a)–(f) with the parameters α and β and the contact angles.

3.2. Bubble formation on a hydrophilic surface

We now examine the bubble formation in a nanochannel with hydrophilic surfaces. Due to the nanoscale of the separate distance of the solid walls, the effect of wall adsorption on the bulk density of the liquid is very prominent at the hydrophilic surfaces.

Fig. 4 shows bubble formation in a nanochannel with strong hydrophilic surfaces ($\alpha = 1$ and $\beta = 1$) with the initial liquid density of $\rho_l = 0.6\rho_{lsat}$ (left) and $\rho_l = 0.833\rho_{lsat}$ (right). For both cases, it is found that the bubble appears in the bulk liquid, at some distance from the adsorption layer near the solid surface. For the case of $\rho_l = 0.833\rho_{lsat}$,

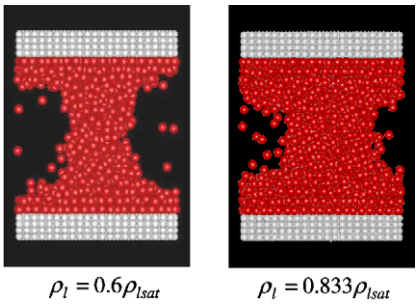

Fig. 4. Bubble in a nanochannel with hydrophilic surfaces (a) of $\alpha = 1$, $\beta = 1$. $\rho_l = 0.6\rho_{lsat}$; $\rho_l = 0.833\rho_{lsat}$.

Table 1
Simulation Cases (a)–(f) in Fig. 3 and corresponding contact angles

Simulation cases	(a)	(b)	(c)	(d)	(e)	(f)
α	1	0.5	0.14	0.14	0.14	0.14
β	1	1	1	0.5	0.3	0.1
θ (°)	0	0	0	95	150	180
Surface wettability	Strongly hydrophilic	Middle hydrophilic	Weak hydrophilic	Weak hydrophobic	Middle hydrophobic	Strong hydrophobic

adding the driving force at the inlet results in a two-phase flow at the center of the channel, while the layer of liquid adjacent to the wall keeps its strong adsorption to the solid atoms under the imposed driving force. This means that the solid–liquid interface has large hydrodynamic resistance and thus, the flow moves very slowly and no-slip boundary condition is valid in this case.

For the surface with weak hydrophilic interaction ($\alpha = 0.14$ and $\beta = 1$), a bubble is found in the bulk liquid for the initial liquid density of $\rho_l = 0.6\rho_{lsat}$ (see Fig. 5a). However, for the initial liquid density of $\rho_l = 0.833\rho_{lsat}$, no bubble was observed in the channel full of liquid as shown in Fig. 6a. As mentioned earlier, the liquid in this case ($\rho_l = 0.833\rho_{lsat}$) is in the metastable state (see Fig. 2) and phase change may occur only by disturbance to the system. It is found that a bubble generates in the bulk liquid within the first 100 ps during the NEMD simulation after the driving force is imposed. The bubble growing process is illustrated in Fig. 6b and c. During the first 50 ps of the NEMD simulation, density of liquid fluctuates and the liquid begins to flow due to the driving force. An embryo is observed after 50 ps shown in Fig. 6b and it grows to a vapor bubble within the following 50 ps shown in Fig. 6c. Further run for 1900 ps shows that the bubble stops growing and its size is maintained at $r = 1$–2 nm in the two-phase flow. It is considered that the disturbance of the driven force may cause a localized region with low liquid density. The molecular collisions will increase the local translational energy if the density is low enough. Where atoms with large energy gather around, then the vapor embryo is generated. Therefore, the bubble is sustained by the surrounding atoms at the curved liquid–vapor interface with large energy.

3.3. Bubble formation on a hydrophobic surface

In the case of the hydrophobic surface with weak interaction ($\alpha = 0.14$, $\beta = 0.5$), heterogeneous nucleation is considered next. As shown in Fig. 5b and c, a bubble is found for the initial liquid density of $\rho_l = 0.6\rho_{lsat}$, which appears on the hydrophobic surface directly with a hemispherical shape. Since the initial liquid density of $\rho_l = 0.833\rho_{lsat}$ is in a metastable state, it is found that a bubble generates at the solid–liquid interface within the first 100 ps after adding the driving force as shown in Fig. 7c. Comparing with the case of hydrophilic surface showing in Fig. 6, the bubble is smaller but in a hemispherical shape. The behavior of the nucleation on a hydrophobic surface clearly differs from that of the hydrophilic surface: the heterogeneous nucleation is caused by the collisions of liquid to the solid atoms. Also, the liquid adjacent to the solid wall is little dense and velocity slip occurs at the boundary in this case.

For the non-wetting surface with $\alpha = 0.14$, $\beta = 0.1$, the result shows that a gap always exists between the liquid and the solid surface as shown in Fig. 5c for the case of initial $\rho_l = 0.6\rho_{lsat}$. It is found that no bubble appears in the nanochannel with non-wetting surfaces. Apparent velocity slip is observed at the boundary and the velocity profile normalized to the flow direction is of a plug flow shape [2].

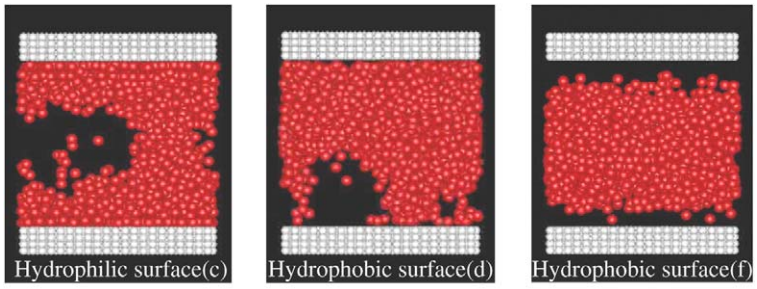

Fig. 5. Comparisons of nucleation behavior with different interface wettability at initial $\rho_l = 0.6\rho_{lsat}$; (a) $\alpha = 0.14$, $\beta = 1$; (b) $\alpha = 0.14$, $\beta = 0.5$; (c) $\alpha = 0.14$, $\beta = 0.1$.

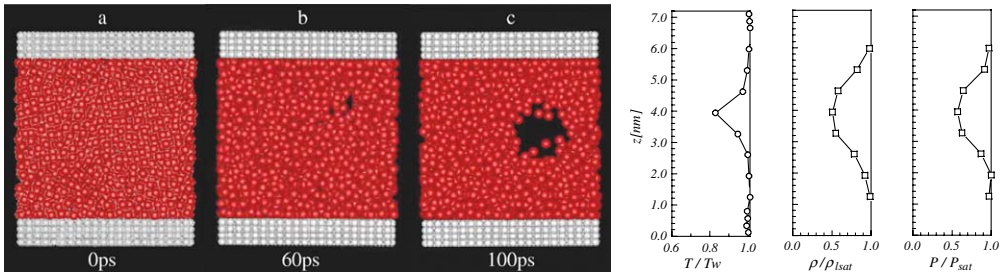

Fig. 6. Bubble formation in a nanochannel with hydrophilic surfaces (c) of $\alpha = 0.14$, $\beta = 1$ from initial metastable state ($\rho_l = 0.833\rho_{lsat}$) with driving force at the inlet.

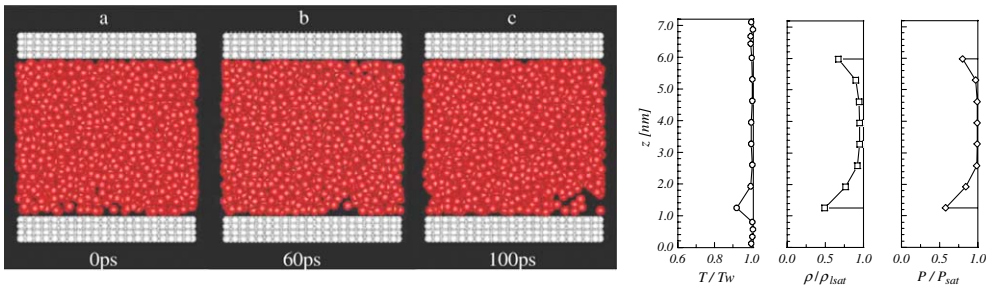

Fig. 7. Bubble formation in a nanochannel with hydrophobic surfaces (d) of $\alpha = 0.14$, $\beta = 0.5$ from initial metastable state ($\rho_l = 0.833\rho_{lsat}$) with driving force at the inlet.

3.4. Temperature and pressure profiles in the nanochannel

The local data of temperature, pressure and density along the z-direction during a simulation time of 500 ps (the details are described elsewhere [2]) were also collected. The temperature profile along the z-direction is reduced by the wall temperature of 100 K and the pressure, density profiles are compared with the saturation properties at 100 K. The results are shown at the right side of Fig. 6 for the hydrophilic surface and Fig. 7 for the hydrophobic surface. It is shown that the temperature is almost uniform in the bulk liquid, but is low in the area where bubble nucleation takes place. This is considered to be the reason that there are few vapor atoms in the bubble as confirmed from the density profiles. Therefore, the pressure profile shows a trend similar to the density distribution.

3.5. Comparison with the Young–Laplace Equation

From the classical point of view, the bubble is considered to generate from a "critical size" and nucleation can proceed at fairly low levels of gas superheat once gas cavities exist on a substrate surface [6,7]. Consider the simplest case of homogenous nucleation, i.e., a bubble existing in pure liquid in a stable equilibrium situation as shown in Fig. 8. The Young–Laplace equation requires that the vapor pressure inside bubble P_v is higher than the liquid pressure P_l due to the surface tension σ of vapor–liquid interface.

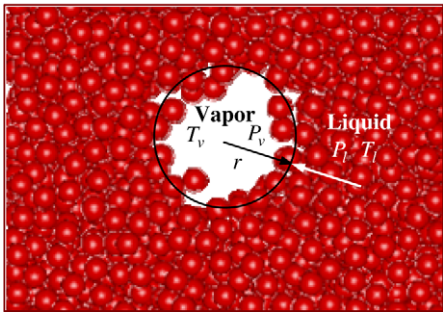

Fig. 8. Force balance on an embryo vapor bubble in pure liquid.

$$P_v - P_l = \frac{2\sigma}{r}, \tag{4}$$

where r is the radius of the bubble. Applying the Clausius–Clapeyron equation:

$$P_s - P_l = \frac{T_v - T_{sat}}{T_{sat}} \cdot \frac{h_{fg}}{\upsilon'' - \upsilon'} \tag{5}$$

to Eq. (4), the required liquid superheat ΔT_s is

$$\Delta T_s = T_v - T_{sat} = \left(\frac{1}{\rho_v} - \frac{1}{\rho_l}\right)\frac{T_{sat}}{h_{fg}} \cdot \frac{2\sigma}{r}. \tag{6}$$

Here, T_v is the temperature of vapor, T_{sat} is the saturation temperature corresponding to P_l, υ'' and υ' are the specific volume of vapor and liquid, ρ_v is the vapor density and ρ_l is the liquid density, h_{fg} is enthalpy of evaporation. Since the pressure difference of $P_v - P_l$ and the superheat ΔT_s are proportional to $1/r$, it results in $(P_v - P_l) \Rightarrow \infty$ or $\Delta T_s \Rightarrow \infty$ as $r \Rightarrow 0$.

Based on the molecular dynamics simulation described in the previous sections, it is clear that the bubble is generated from a size smaller than one nanometer through the space between the liquid atoms or liquid–solid atoms in collisions. Also, the pressure and temperature in a nanobubble is lower than those given by Eqs. (4) and (6). Eq. (4) for bubble formation is based on a hypothesis that the bubble is full of vapor atoms and thus, the force inside the bubble is in balance with that outside of the bubble. However, this hypothesis is not applicable in the case of a nano-size bubble. As seen from the snapshot shown in Fig. 8, few vapor atoms are inside the nanobubble. The present work suggests that Eq. (4) may be inadequate to explain the nanobubble formation. In disagreement with the prediction of the Young–Laplace equation, we suggest that the force balance for nanobubble is supported with the curved liquid–vapor interface instead of the vapor inside nanobubble. That is, the liquid–vapor interface plays an important role on the force balance of nanobubble.

4. Conclusions

Bubble nucleation dynamics for a liquid confined in nanochannels based on molecular dynamics simulations has been studied in this paper. The following conclusions may be drawn from the present study:

1. The bubble nucleation behavior is remarkably different at surfaces with different wettabilities. The nucleation at the hydrophilic surface is of homogeneous type, while heterogeneous type is found at the hydrophobic surface. No bubble nucleation will take place on a non-wetting surface.
2. The Young–Laplace equation may be inadequate to describe a nanobubble since there is few vapor atoms inside bubble to support a force balance with the surrounding liquid.

Acknowledgements

The first two authors (G. Nagayama and T. Tsuruta) wish to thank the Ministry of Education, Science and Culture of the Japanese Government for the support of this work through the Grant-in Aid for Scientific Research, Project No. 16656074, and the third author (P. Cheng) wishes to thank the National Natural Science Foundation of China for partial support of this work through Grant No. 50536010.

References

[1] H.Y. Wu, P. Cheng, An experimental study of convective heat transfer in silicon microchannels with different surface conditions, Int. J. Heat Mass Transfer 46 (2003) 2547–2556.
[2] G. Nagayama, P. Cheng, Effects of interface wettability on microscale flow by molecular dynamics simulation, Int. J. Heat Mass Transfer 47 (2004) 501–513.
[3] V. Dupont, M. Miscvic, J.L. Joly, V. Platel, Boiling incipience of highly wetting liquids in horizontal confined space, Int. J. Heat Mass Transfer 46 (2003) 4245–4256.
[4] J.W. Yang, J.M. Duan, D. Fornasiero, J. Ralston, Very small bubble formation at the solid–water interface, J. Phys. Chem. B 107 (2003) 6139–6147.
[5] P. Deng, Y.K. Lee, P. Cheng, The growth and collapse of a microbubble under pulse heating, Int. J. Heat Mass Transfer 46 (2003) 4041–4050.
[6] L.S. Tong, Y.S. Tang, Boiling Heat Transfer and Two-Phase Flow, Taylor & Francis, Washington DC, 1997.
[7] V.P. Carey, Liquid–Vapor Phase-Change Phenomena: An Introduction to the Thermophysics of Vaporization and Condensation Processes in Heat Transfer Equipment, Taylor & Francis, Bristol PA, 1992.
[8] T. Kimura, S. Maruyama, Molecular dynamics simulation of heterogeneous nucleation of a liquid droplet on a solid surface, Microscale Thermophys. Eng. 6 (2002) 3–13.
[9] S. Maruyama, T. Kimura, A molecular dynamics simulation of a bubble nucleation on solid surface, Int. J. Heat Technol. 8 (2000) 69–74.
[10] S. Maruyama, T. Kimura, M.C. Lu, Molecular scale aspects of liquid contact on a solid surface, Therm. Sci. Eng. 10 (2002) 23–29.
[11] T. Kinjo, M. Matsumoto, Cavitation processes and negative pressure, Fluid Phase Equilib. 144 (1998) 343–350.
[12] M. Matsumoto, K. Miyamoto, K. Ohguchi, et al., Molecular dynamics simulation of a collapsing bubble, Progr. Theor. Phys. Suppl. 138 (2000) 728–729.
[13] T. Kinjo, G.T. Gao, X.C. Zeng, Bubble nucleation in confined liquids: Molecular dynamics study, Progr. Theor. Phys. Suppl. 138 (2000) 732–733.
[14] K. Yasuoka, M. Matsumoto, Molecular dynamics of homogeneous nucleation in the vapor phase. I. Lennard-Jones fluid, J. Chem. Phys. 109 (1998) 8451–8462.
[15] K. Yasuoka, M. Matsumoto, Molecular dynamics of homogeneous nucleation in the vapor phase. II. Water, J. Chem. Phys. 109 (1998) 8463–8470.
[16] J.G. Weng, S. Park, C.L. Tien, Interfacial ambiguities in microdroplets and microbubbles, Microscale Thermophys. Eng. 4 (2000) 83–87.
[17] M.P. Allen, D.J. Tildesley, Computer Simulation of Liquids, Oxford University Press, New York, 1987.
[18] R.J. Sadus, Molecular Simulation of Fluids, Elsevier, Netherlands, 1999.
[19] X.D. Din, E.E. Michaelides, Kinetic theory and molecular dynamics simulations of microscopic flows, Phys. Fluids 9 (1997) 3915–3925.
[20] J.-L. Barrat, L. Bocquet, Large slip effect at a nonwetting fluid–solid interface, Phys. Rev. Lett. 82 (1999) 4671–4674.
[21] J. Delhommelle, P. Millie, Inadequacy of the Lorentz–Berthelot combining rules for accurate predictions of equilibrium properties by molecular simulation, Mol. Phys. 99 (2001) 619–625.